Landslides (2023) 20:143–156
DOI 10.1007/s10346-022-01959-8
Received: 10 November 2021
Accepted: 18 August 2022
Published online: 5 September 2022

Mohammad Heidarzadeh · Hiroko Miyazaki · Takeo Ishibe · Hiroshi Takagi · Ramtin Sabeti

Field surveys of September 2018 landslide-generated waves in the Apporo dam reservoir, Japan: combined hazard from the concurrent occurrences of a typhoon and an earthquake

Abstract We report and analyze a case study of landslide-generated waves that occurred in the Apporo dam reservoir (Hokkaido, Japan) culminating from the rare incident of hazard combination from the September 2018 Typhoon Jebi and Hokkaido earthquake (M_w 6.6 on 5 September 2018). The typhoon and earthquake were concurrent and produced thousands of landslides in the area by the combined effects of soil saturation and ground acceleration. Here, we report the results of our field surveys of the landslides that occurred around the Apporo dam and generated damaging waves in the reservoir. We identified six landslides at a close distance to the dam body; the largest one has a length of 330 m, a maximum width of 140 m and a volume of 71,400 m^3. We measured wave runup at a single point with height of 5.3 m for the landslide-generated wave in the reservoir and recorded the damage made to the revetments at the reservoir banks. By considering the locations of the landslides and their potential propagation paths, we speculate that possibly three of the six surveyed landslides contributed to the measured wave runup. The surveyed runup was reproduced by inputting landslide parameters into two independent empirical equations; however, other independent empirical relationships failed to reproduce the observed runup. Our field data from the Apporo dam can be used to improve the quality of predictions made by empirical equations and to encourage further research on this topic. In addition, our field data serves as a call for strengthening dams' safety to landslide-generated waves in reservoirs.

Keywords Earthquake · Typhoon · Landslide · Landslide impulse wave · Hydraulics · Dam engineering · Hazard combinations

Introduction

The Atsuma area of Hokkaido (Japan) was the site of thousands of destructive landslides on 5 September 2018 (UTC) triggered by an M_w 6.6 earthquake. According to the United States Geological Survey (USGS), this reverse-faulting earthquake occurred at 42.686°N, 141.929° E with an origin time of 18:07:59 (UTC) and a focal depth of 35.0 km (Fig. 1a). Nearly six thousand landslides were reported in the area, taking the lives of 36 people (Yamagishi and Yamazaki 2018; Zhang et al. 2019; Aimaiti et al. 2019). The earthquake was approximately concurrent with the passage of Typhoon Jebi over Hokkaido, which brought torrential rainfall in the area and saturated soils on mountain slopes before the earthquake occurrence (Le et al. 2019; Aimaiti et al. 2019). Typhoon Jebi, which was active over Japan in the period 3–6 September 2018, was the strongest typhoon to hit Japan since 1993 and caused severe destruction and 13 deaths (Le et al. 2019; Heidarzadeh and Rabinovich 2021).

Following the September 2018 Hokkaido earthquake, landslide-generated waves were generated in the Apporo dam reservoir, which produced some damage to reservoir banks. The hazard from landslide-generated waves in dam reservoirs has been long known (e.g., Schnitter 1964; Schuster and Wieczorek 2002; Ataie-Ashtiani and Yavari-Ramshe 2011; Ersoy et al. 2019; Evers et al. 2019a, b; Evers and Boes 2019). One of the most destructive landslide-generated waves worldwide occurred in the Vajont dam reservoir (Italy) in October 1963 killing more than 2000 people (Bosa and Petti 2011; Vacondio et al. 2013; Roberts et al. 2014). Miyagi et al. (2011) reported a large landslide (volume of more than 67 million m^3) that occurred in the Aratozawa Dam area (Tohoku, Japan) in June 2008 following an M7.2 earthquake. Roberts et al. (2013) reported a landslide-generated impulse wave in Chehalis Lake, Canada in December 2007 due to the failure of a 3 million m^3 rockmass. Some other similar destructive incidents include: Pontesei dam (Italy) incident in 1959 (Panizzo et al. 2005), Three Gorges Reservoir (China) incidents in 2003, 2008 and 2015 (Huang et al. 2012; Yin et al. 2015; Zhou et al. 2016); the 2008 San Juan de Grijalva landslide (Alcantara-Ayala and Dominguez-Morales 2008); and Lake Lucerne in Switzerland in June 2007 (Evers et al. 2019a). Hermanns et al. (2014) and Roberts et al. (2014) provided reviews of regional and global incidents, respectively. An important aspect of the landslide-generated waves in the Apporo dam reservoir is the occurrence of multiple landslides, which potentially increases hazard magnitude. Other worldwide incidents of multiple landslides in a dam reservoir or fjord are the 2007 Aysen Fjord, Chile (Oppikofer et al. 2019), the 2018 Palu event within the Palu bay, Indonesia (Takagi et al. 2019; Heidarzadeh et al. 2019), and the 1964 incident in Kenai Lake, Alaska (USA) (McCulloch 1966). The Indonesian event involved both subaerial and submarine landslides.

In this study, we report results of our field surveys of the evidence of landslide-generated waves in the Apporo dam reservoir following the September 2018 Hokkaido earthquake. In order to contribute to the safety of dams worldwide, it is critically important to report and analyze any incident of landslide-generated waves in dam reservoirs. The authors visited the Apporo dam area in the period 29 May–4 June 2019 to conduct field surveys of the landslide-generated waves. Here, we report our field survey results, analyze them, and compare the measured landslide-generated wave runup height with those obtained using existing empirical equations.

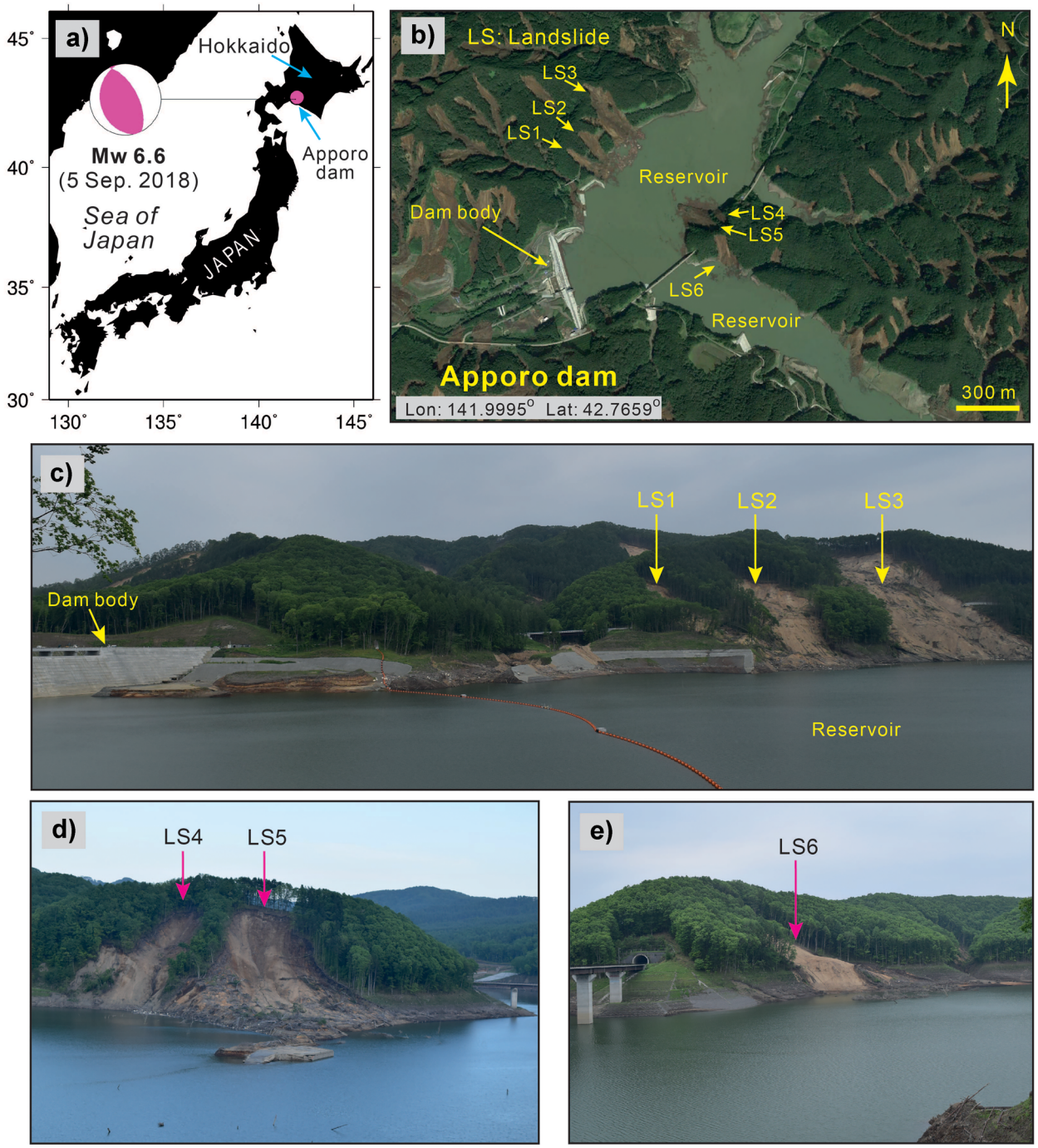

Fig. 1 **a** Location of the Apporo dam and reservoir in Hokkaido, Japan, and the epicenter of the earthquake. **b** A satellite image from Google-Earth (https://earth.google.com/) showing the dam area after the earthquake and the location of six landslides (LS1–LS6) near the dam body. **c**–**e** Our field photos showing detailed views from the six landslides near the dam body. LS is an acronym for "landslide"

Background information

Apporo dam in Hokkaido, Japan

Apporo dam is a trapezoidal cemented sand and gravel (CSG) dam located in Hokkaido (Figs. 1 and 2), which was built for flood control and supplies water for irrigation and domestic uses. The dam construction was completed in 2019. The CSG dam is a relatively new type of dam construction technology, which was developed in Japan and offers benefits such as its environment-friendly construction materials, higher dam stabilities and low maintenance costs (Japan Commission on Large Dams 2018). In principle, a CSG

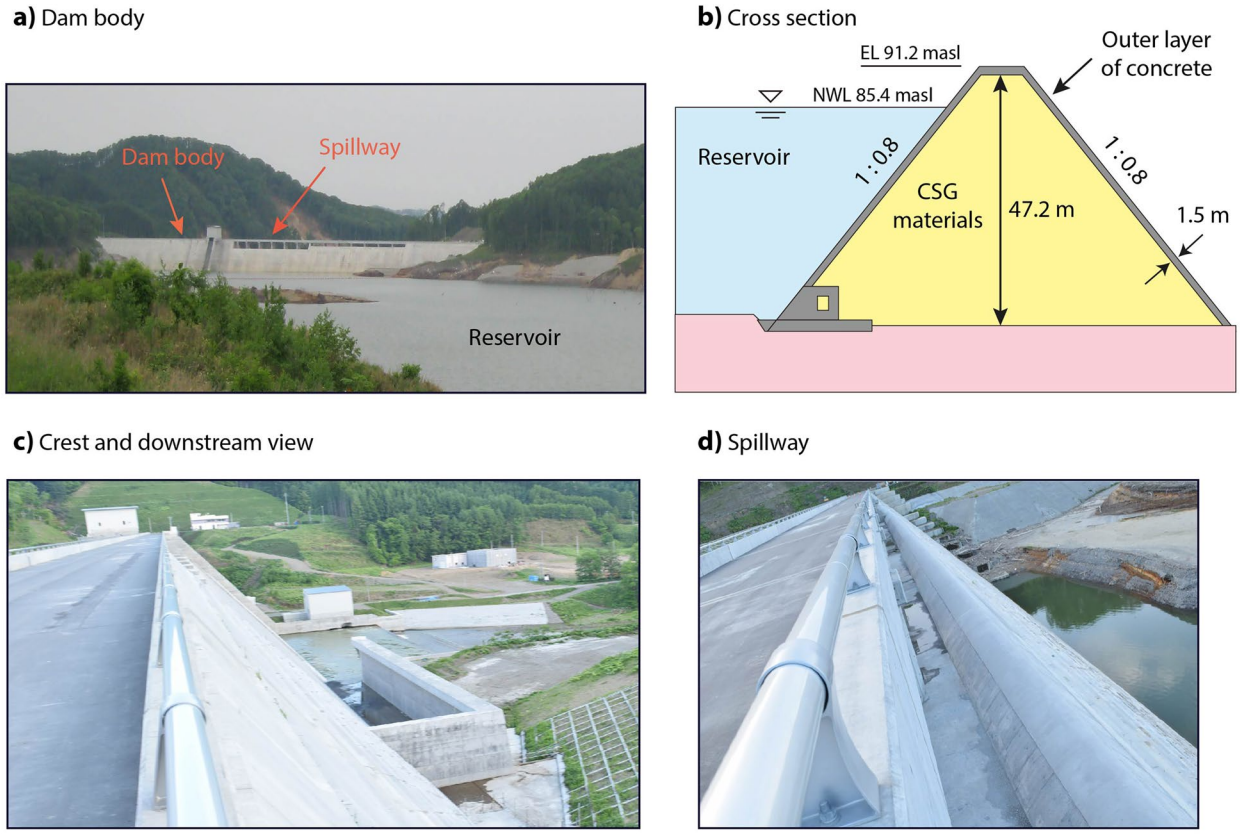

Fig. 2 Apporo dam located in Hokkaido, Japan. **a** A field photo showing the dam body and the reservoir. **b** A cross section of the dam showing that the dam is constructed from cemented sand and gravel (CSG) with a 1.5 m concrete layer at the outer layer. This sketch is based on the dam body drawings provided to the first author by the site engineers during the surveys. **c** A view of the dam crest and the downstream area. **d** The entrance of the spillway. In **b**, EL, NWL, and masl are abbreviations for "elevation," "normal water level," and "meters above the sea level," respectively

dam is a type of gravity dam that comprises a trapezoid body filled with CSG materials, which are relatively cheap and can be rapidly constructed with relatively simple technologies. The dam body is protected by a concrete layer at its face on all sides with a thickness of 1.5 m (Fig. 2b). The Apporo dam has a height of 47.2 m, a crest length of 516 m, a dam body volume of 480,000 m^3, reservoir water volume of 47.4 million m^3, and reservoir surface area of 3.03 million m^2 (Japan Commission on Large Dams 2018). The dam is equipped with an Ogee-type spillway (e.g., Savage and Johnson 2001) fitted in the middle of the dam body (Fig. 2a and d). The CSG material used for the dam body is shale, and the dam foundation is made of alternate layers of shale and shale-sandstone.

Interactions of the September 2018 Typhoon Jebi and Hokkaido earthquake

The purpose of this section is to add insights into the origin of extraordinary landslide activities in the Atsuma area through analyzing earthquake and typhoon data and their timings. The data used for this analysis are the earthquake mainshock and aftershock information, the rainfall data, and typhoon pressure field. Earthquake data belong to a period of one month after the mainshock (i.e., 5 September–5 October 2018) and are provided by the unified earthquake catalogue of Japan Meteorological Agency (https://www.data.jma.go.jp/svd/eqev/data/bulletin/hypo.html). For earthquake focal mechanisms, we used the focal mechanism catalogue of the Global Centroid Moment Tensor (GCMT) project (Dziewonski et al. 1981; Ekström et al. 2012). The data of rainfall and typhoon pressure field are from the Automated Meteorological Data Acquisition System (AMeDAS) of the Japan Meteorological Agency (https://www.jma.go.jp/jma/en/Activities/amedas/amedas.html).

Rainfall and Typhoon Jebi's pressure field are shown in Fig. 3. Typhoons that make landfall in Japan usually rapidly lose their energy and become tropical depressions, but Typhoon Jebi maintained a typhoon-status intensity with its central pressure of 975 hPa (hectopascal) and maximum wind speed of 50 knots (25.7 m/s) when it approached Hokkaido (Fig. 3b). This caused a band of heavy rainfall along the path of the typhoon (Fig. 3c). The rainfall in this area was relatively heavy from June to September 2018. Since the event occurred in the summertime with hot weather and sunny days, the surfaces of the mountain tended to be dry, but the deeper part (deeper than 10–20 cm) of the ground is assumed to be wet. In addition, Typhoon Jebi caused heavy rainfall in the vicinity of Atsuma. In particular, Typhoon Jebi's daily rainfall was 12–14 mm in the Atsuma region immediately before the earthquake

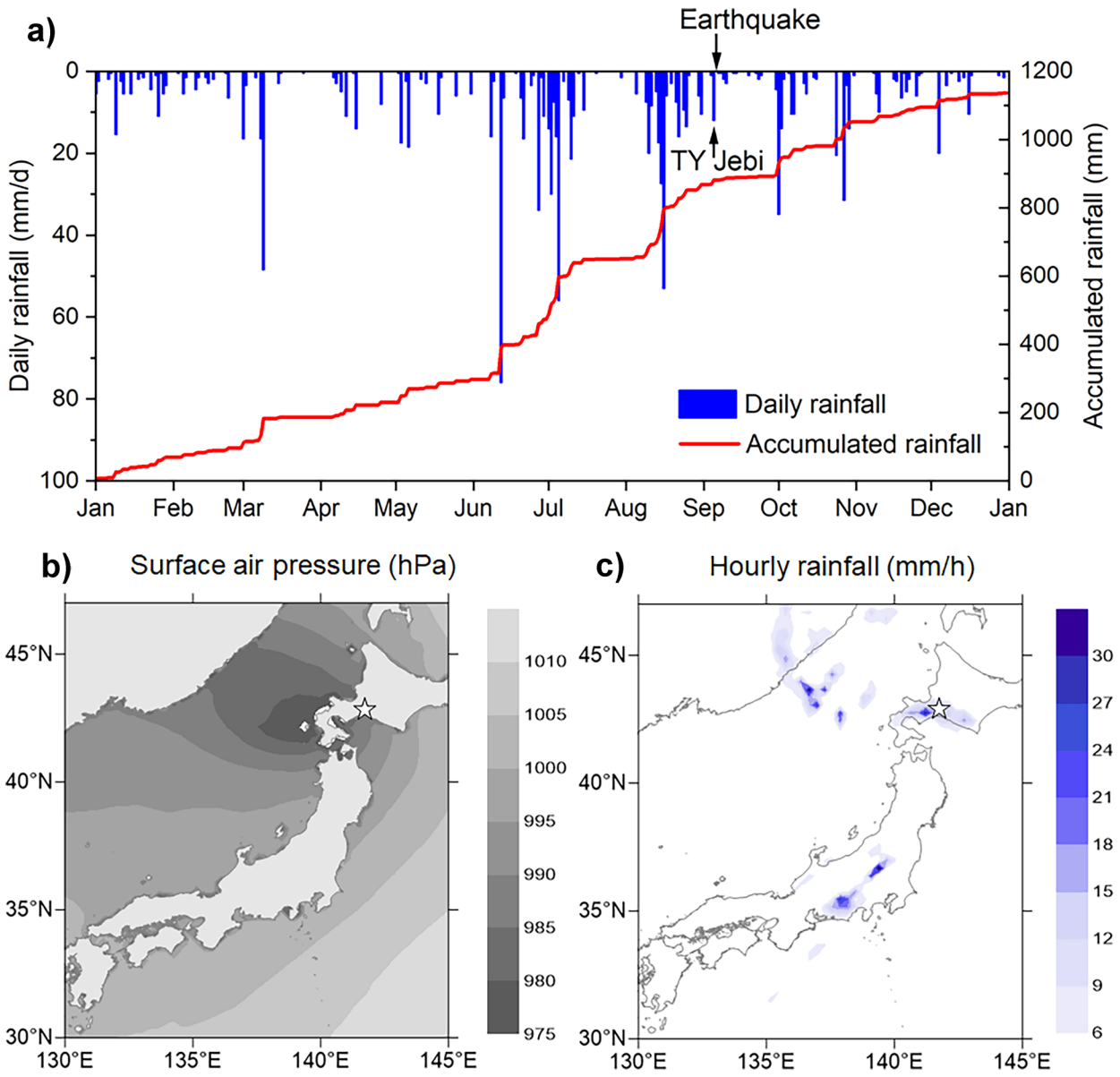

Fig. 3 **a** Rainfall records at Atsuma meteorological station operated by JMA spanning 2018. The times of the earthquake and Typhoon Jebi are marked in the figure by arrows. **b** Surface air pressure at the time of Typhoon Jebi's approach to Hokkaido (17:00 UTC on 4 September 2018). **c)** Rain band induced by the Typhoon Jebi. The stars in **b** and **c** indicate the location of Atsuma Town. Surface air pressure and rainfall data are extracted using the typhoon model with the meso-scale weather forecasting model of the Japan Meteorological Agency (JMA-MSM) (Takagi and Takahashi 2021)

(arrows in Fig. 3a), which most likely was sufficient to entirely saturate the mountains and make them susceptible to sliding.

The distribution of aftershocks of the earthquake (Fig. 4a) shows that the Apporo dam is located within the intensive aftershock activity zone. The total length of the intensive aftershock zone is approximately 32 km which begins from around the coastline (latitude 42.55°) and extends to the north until approximately latitude 42.83°. The dam is located approximately 9 km to the north of the mainshock epicenter (Fig. 4a). Detailed analyses from the relocated aftershocks by using data from a permanent local seismic network revealed that the aftershock depths were concentrated at the depth of 20–40 km (Katsumata et al. 2019). Magnitude-time distribution of the aftershocks and their cumulative number (Fig. 4b) show steady growth of aftershocks during the 30 days following the mainshock.

Among other factors, landslides occur following heavy rainfall, such as many landslides that occurred in Dominica following the 2017 Hurricane Maria (Heidarzadeh et al. 2018), or following ground shaking induced by earthquakes, such as landslide activities in Palu (Indonesia) following the September 2018 earthquake (Takagi et al. 2019) and other events (e.g., Heidarzadeh and Satake 2015; Tsuji et al. 2011; Heidarzadeh et al., 2022). The landslides in the Atsuma

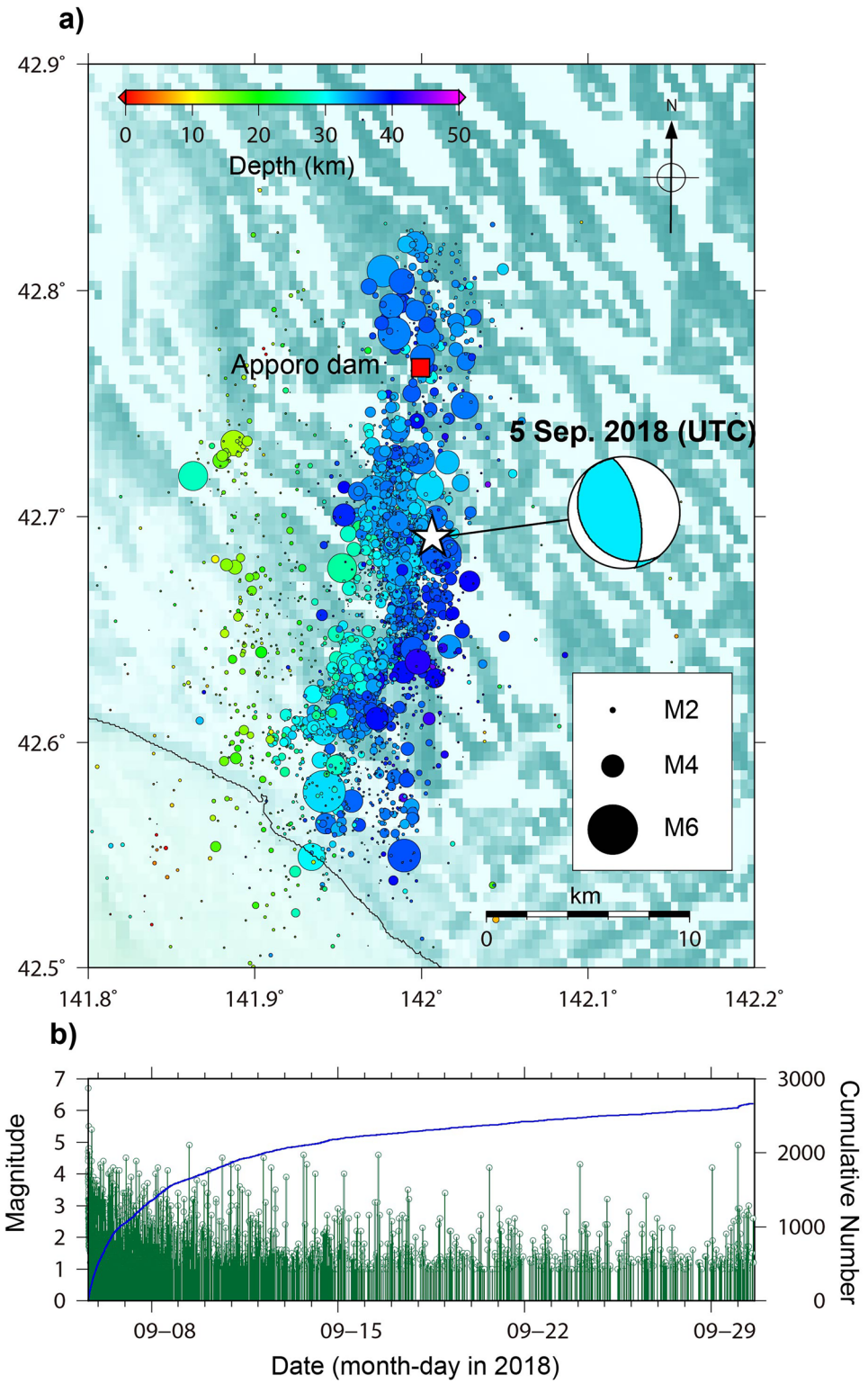

Fig. 4 The mainshock and one-month aftershocks (M1 or larger) of the 5 September 2018 Hokkaido M_w 6.6 earthquake around the Apporo dam. **a** Distribution of the one-month aftershocks and the mainshock in the region relative to the dam site. **b** Magnitude-time plot indicated by the left vertical axis and the green bars and circles. The right vertical axis and the thick blue curve indicate the cumulative number of aftershocks. The horizontal axis begins from the earthquake origin time (i.e., 5 September 2018 UTC). Star shows the epicenter of the earthquake

region in September 2018 occurred due to the combined effects of typhoon rainfall and earthquake shaking. Although it is a challenge to precisely quantify the contribution of each trigger to landslide initiation, the extraordinary landslide occurrences in the region can be explained by the combined effects of the earthquake and the typhoon. Such destructive hazard combinations and interactions were discussed by several authors (e.g., Gill and Malamud 2016; Liu et al. 2016; Lyddon et al. 2019; Adams and Heidarzadeh 2021; Heidarzadeh and Feizi, 2022). Gill and Malamud (2016) presented three types of relationships among interacting hazards which are: increased probability, triggering, and catalysis (i.e., wet soils due to heavy rainfall at the time of the earthquake increased the number

and extent of landslides). For the case of the 2018 Atsuma landslide incident, the two primary hazards (i.e., the earthquake and the typhoon) are completely independent and neither of them was the triggering mechanism for the other. However, they worked together to trigger a secondary hazard (i.e., the landslides), increased landslide probability and catalyzed it. In fact, the 2018 Atsuma landslide disaster, with 36 deaths, is a rare case that involves all three mechanisms (i.e., increased probability, triggering, and catalysis).

Landslide activities following the Typhoon Jebi and Hokkaido earthquake

Landslide activity and characteristics following the September 2018 Hokkaido earthquake have been studied by several authors. According to Yamagishi and Yamazaki (2018), the geology of the area is Neogene sedimentary rocks covered by air-fall lapilli-sized pumice (9000 years ago) with maximum surface thickness of 4–5 m. Yamagishi and Yamazaki (2018) found that the majority of the landslides were shallow planar landslides, with a few meters of depth, and they initiated within the pumice layer. During our field surveys, we also observed that most of the landslides around the Atsuma area were shallow with an average depth of approximately 2–3 m (Fig. 5). Satellite data analyses by Aimaiti et al. (2019) provided a tool to map the co-seismic landslides. Zhang et al. (2019) reported that most of the landslides occurred in areas with modified Mercalli intensity of 7–8 with peak ground acceleration in the range from 0.4 g to 0.7 g, where g is gravitational acceleration (= 9.81 m/s^2). The slope angles of the landslides were between 15° and 35° (Zhang et al. 2019). According to Osanai et al. (2019), some large-scale and deep-seated landslides also were generated, including a landslide that formed a landslide dam in the area. Wang et al. (2019) identified 7837 landslides with a total volume of 23–38 million m^3 of deposits. Other authors who studied this event include Li et al. (2020), Chang et al. (2021), Chen et al. (2021), and Lu et al. (2021).

Data and methods

The records of reservoir water level and reservoir water volumes are provided by the Hokkaido Prefecture Dam Authority. The time interval of reservoir water level measurements is 10 min. Field data are collected during our fieldworks in the affected area (Hokkaido, Japan). The authors surveyed the Atsuma area, including the Apporo dam site, for field surveys. During the fieldwork, we measured landslide dimensions (i.e., length, width, thickness, elevation) and the runup height of the landslide-generated waves using a TruPulse 200 laser rangefinder (Laser Technologies Inc) (Fig. 6). The sites of the measurements were located by a handheld GPS device of the Garmin model (Garmin Ltd.) for georeferencing the locations. All locations were photographed, and notes were made. The measured value of wave runup height was corrected relative to the reservoir water level at the time of the event (Fritz et al. 2008; Omira et al. 2019; Heidarzadeh et al. 2018, 2020). The reservoir water level at the time of our survey (4 June 2019) was 68.9 masl (meters above the sea level) whereas it was 70.8 masl at the time of the event (5 September 2018; UTC) (Fig. 7). The dimensions of the landslides were used to approximate the volume of the landslides using simple mathematical equations for the volume of geometrical shapes.

We compared the measured runup height of the landslide-generated waves with those obtained using existing empirical equations. The motivation for conducting this comparison was to examine the reproducibility of the field-measured runup height measurements using existing empirical equations and to encourage further research on developing such empirical equations.

Field survey results

We identified six landslides in the vicinity of the dam body through our fieldwork (LS1 to LS6 in Figs. 1 and 6). A summary of landslide dimensions and their volume estimates are presented in Table 1. As previously reported by other authors (e.g., Yamagishi and Yamazaki 2018), most of the landslides in the Atsuma region triggered by the 2018 earthquake were shallow. Our measurements showed that the maximum thicknesses of the landslides were 2–3 m (Fig. 6b). Among the six landslides, the largest landslide is LS3 (Fig. 6e, f) with a length and maximum width of 330 m and 140 m, respectively. The volume of LS3 is estimated at 71.4×10^3 m^3 (Table 1). The landslides displaced the vegetation and tall trees into the reservoir water (Figs. 1 and 6). Debris were found at the other side of the reservoir at the location of wave runup measurement (Fig. 8).

The large amount of displaced soil and vegetation/trees into the reservoir water caused a rapid raise in the reservoir water level (Fig. 7). Immediately after the earthquake occurrence, the reservoir water level started to raise and increased from 70.8 to 71.1 masl (i.e., 0.3 m increase of water level) within approximately 60 min from the earthquake origin time (Fig. 7). The reservoir water volume raised by 0.38 million m^3 based on the recorded rise in the reservoir water level. Although reservoir water volume changes provide important data on the intrusion of landslide materials into the reservoir, it is a challenge to solely associate the water volume raise to the landslides because the reservoir was constantly fed by the river and floods at the time of the incident and there were other coincident landslides in the reservoir far from the dam body. Table 1 shows that the total volume of all six landslides (LS1–LS6) is approximately 0.19 million m^3 (i.e., 190.7×10^3 m^3), which is around half of the reservoir water volume increase.

Data from our surveys revealed that the intrusion of the subaerial landslides into the reservoir was associated with landslide-generated waves in the reservoir. A clear sign of such waves was observed at a narrow opening of the reservoir around the left abutment of the dam (Figs. 8 and 9). At this location, we observed a chaotic pile of woody debris (Fig. 8) and damage to the concrete revetment (Fig. 9). The damage to the concrete revetment can be possible only by powerful waves. This observation was confirmed through discussions with site engineers during our surveys who verified that such damage to the revetment and the tree debris was non-existent before the earthquake. Due to the relatively long sampling interval of reservoir water level measurements (i.e., 10 min), it is not possible to see traces of transient water waves generated by the landslides as such waves normally have a wave period of less than 1 min or up to a few minutes for the potential consequent oscillations for large reservoirs. Figure 7 confirms that such transient water waves or potential consequent oscillations are not recorded due to the long sampling interval of the water level data. As compared to other similar incidents worldwide, such landslide-generated wave damage and high-water marks were reported, for example, during

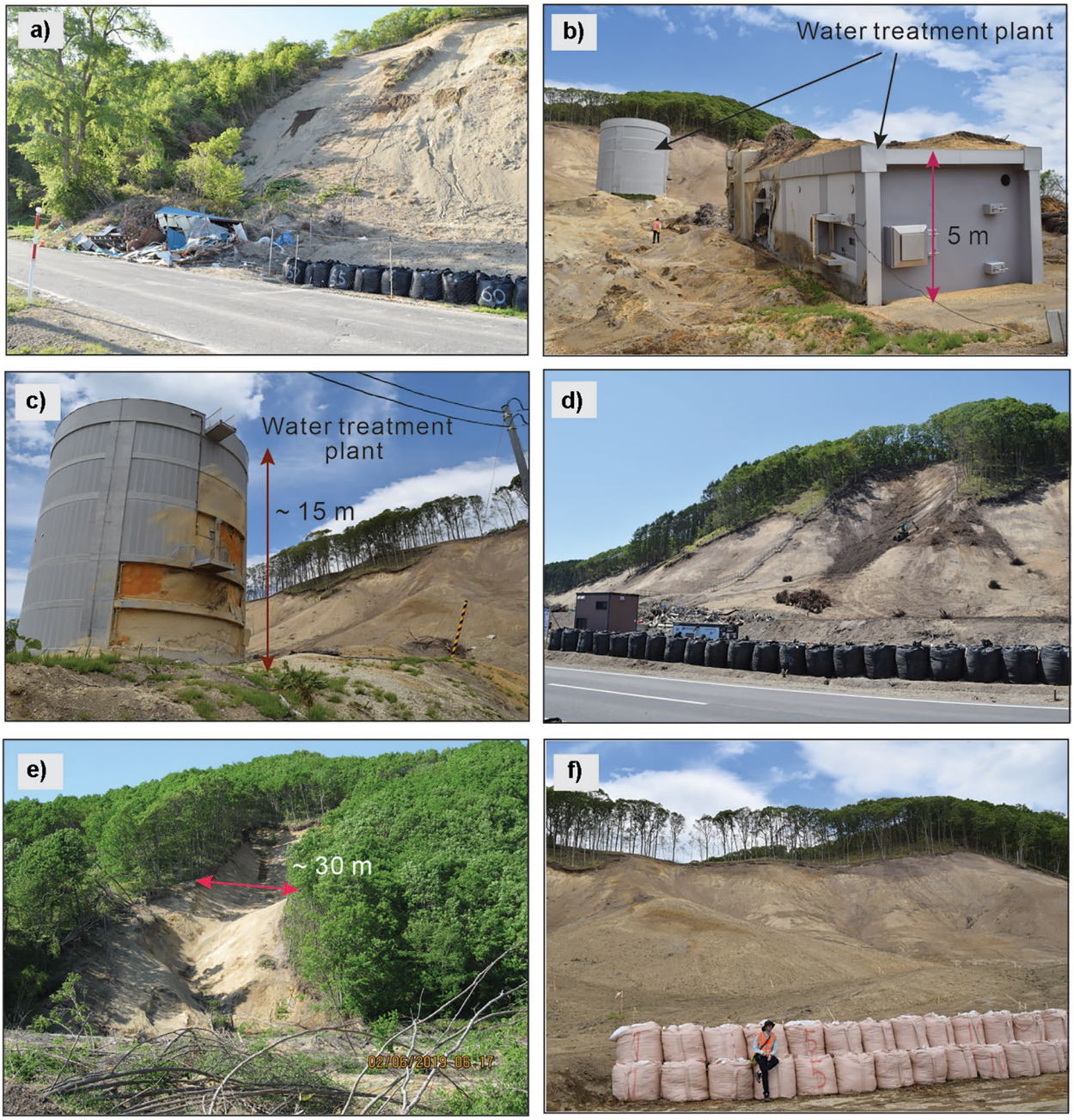

Fig. 5 Field survey photos of landslides following the September 2018 earthquake around the Atsuma area of Hokkaido (Japan). **a** A shallow landslide near a road. **b**, **c** A water treatment plant destroyed by a landslide on a nearby slope. **d** A shallow landslide near a road. **e** A narrow and shallow landslide. **f** A large shallow landslide

the 2007 landslide-generated waves in Chehalis Lake (Canada) as reported by Roberts et al. (2013).

We measured the runup height generated by the landslide-generated waves (parameter "$_R$" in Fig. 8) as 5.3 m. The inundation distance at this location was ~ 80 m. Among the six landslides identified in the vicinity of the dam body, it is likely that only three of them, i.e., LS1, LS2, and LS3, contributed to the wave runup measured at the left abutment of the dam, given the locations of the landslides and the potential propagation paths of the waves. The precise location of the runup measurement point is indicated in the inset of Fig. 8a, b. This runup measurement is only for one single location at the banks of the reservoir and cannot be generalized for other locations. For example, we were unable to measure the runup of landslide-generated waves on the dam body as watermarks were not available on the dam body. However, it would be fair to assume that the wave runups on other locations in the reservoir were of the same order of magnitude (i.e., R = 1 – 10 m) (e.g., Muhari et al. 2019). Therefore, we may conclude that

Fig. 6 **a** Characteristics and dimension estimates of landslides LS1, LS2, and LS3. The background satellite image in panel "a" is from Google-Earth satellite images (https://earth.google.com/) but the dimensions are based on our field surveys. **b**–**f** Our field photos of the landslides from our surveys

although the landslide-generated waves made some damage to the reservoir banks, they were not a major risk for the safety of the dam as the reservoir water level was approximately 20 m below the dam crest elevation at the time of the earthquake (Fig. 7).

Estimating runup heights using empirical equations

It is known that the process of estimating landslide-generated waves using empirical equations is associated with uncertainties. Sabeti and Heidarzadeh (2020) showed that the maximum initial wave amplitude predictions differ up to thousands of times from one empirical equation to another, although they studied only waves generated by submarine landslides. Despite this, it is useful to apply such empirical equations in order to examine their performance and encourage new research on the improvements of such empirical equations.

In this section, we work with three wave parameters: the maximum initial wave amplitude generated by the subaerial landslide (a_M; Fig. 8c), the attenuated wave amplitude due to propagation (a_m; Fig. 8c), and the wave runup height on the reservoir banks (R; Fig. 8c). To estimate a_M, we apply eight independent empirical equations proposed by Fritz et al. (2004), Xue et al. (2019), Heller and Hager (2014), Heller and Spinneken (2015), Slingerland and Voight (1982), Ataei-Ashtiani and Nik-Khah (2008), Noda (1970), and Mohammed and Fritz (2012). There are other equations such as those proposed by Heller and Hager (2010) and McFall and Fritz (2016). It is noted that these equations are a mix of those generated through 2D (e.g., Fritz et al. 2004) and 3D experiments (e.g., Mohammed and Fritz 2012). Some studies have shown that the experiments conducted in 2D may overestimate the wave amplitudes (e.g., Heller and Spinneken 2015).

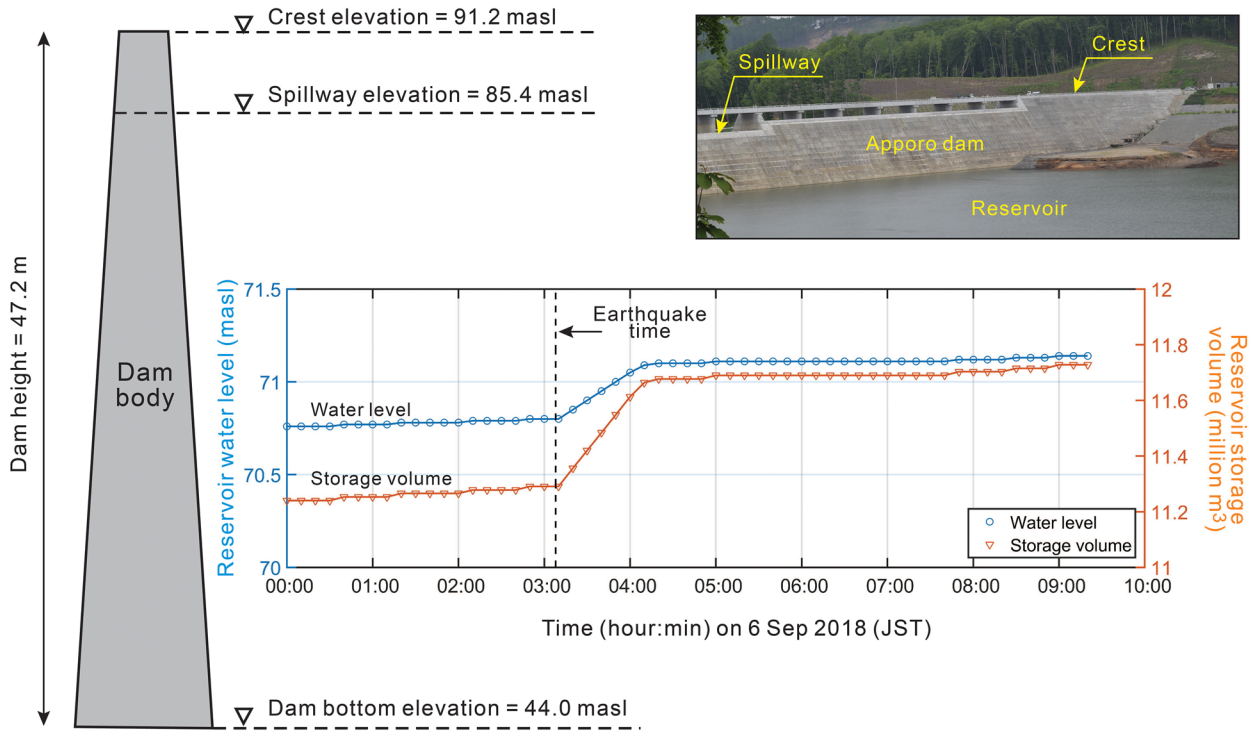

Fig. 7 Temporal variations of reservoir water level (blue) and reservoir storage volume (orange) during the 2018 earthquake and consequent landslides. The vertical dashed line shows the origin time of the earthquake. JST stands for Japan Standard Time. The term "masl" represents "meters above the sea level"

For runup calculations (R), we applied two independent equations by Synolakis (1987) and Evers and Boes (2019), which are obtained through independent physical experiments. Attenuation of the wave due to propagation is considered using the equation proposed by Fritz et al. (2004) by assuming weakly nonlinear oscillatory wave region. The attenuated wave amplitude due to propagation is called a_m here (Fig. 8c, Table 2). For these calculations, we considered the three slides LS1, LS2 and LS3 because potential waves generated by the other three slides were mostly directed outside of the runup measurement point due to their locations. For inputting landslide parameters into the empirical equations, it is assumed that the three landslides LS1, LS2, and LS3 form a combined large landslide and occurred simultaneously although we do not have information about the timing of these landslides. We assumed that the total volume of all landslides contributed to wave generation although it might be the case that some small part of landslide materials might not have entered water. The water depth (h) and slope angle (α) are considered as 27.0 m and 20°, respectively, for all slides in this study.

Table 1 Estimated dimensions and volumes of landslides. See Figs. 1 and 6 for the locations of the landslides. All of these six landslides entered the reservoir, but it is speculated that only three of them (LS1, LS2, and LS3) were responsible for the observed runup

Name of landslide	Slide length (l_s), m	Slide width (b_s), m	Maximum slide thickness (S_{max}), m	Slide volume (V_s), m^3	Slope angle (α), °	Drop heights (Δz), m	Included in wave estimation?
LS1	205	55	2.5	23.3×10^3	20	128	Yes
LS2	200	70	2.5	28.2×10^3	20	104	Yes
LS3	330	140	2.5	71.4×10^3	20	85	Yes
LS4	115	40	2.5	9.7×10^3	20	80	No
LS5	235	75	2.5	35.0×10^3	20	95	No
LS6	175	65	2.5	23.1×10^3	20	65	No
Total				190.7×10^3			

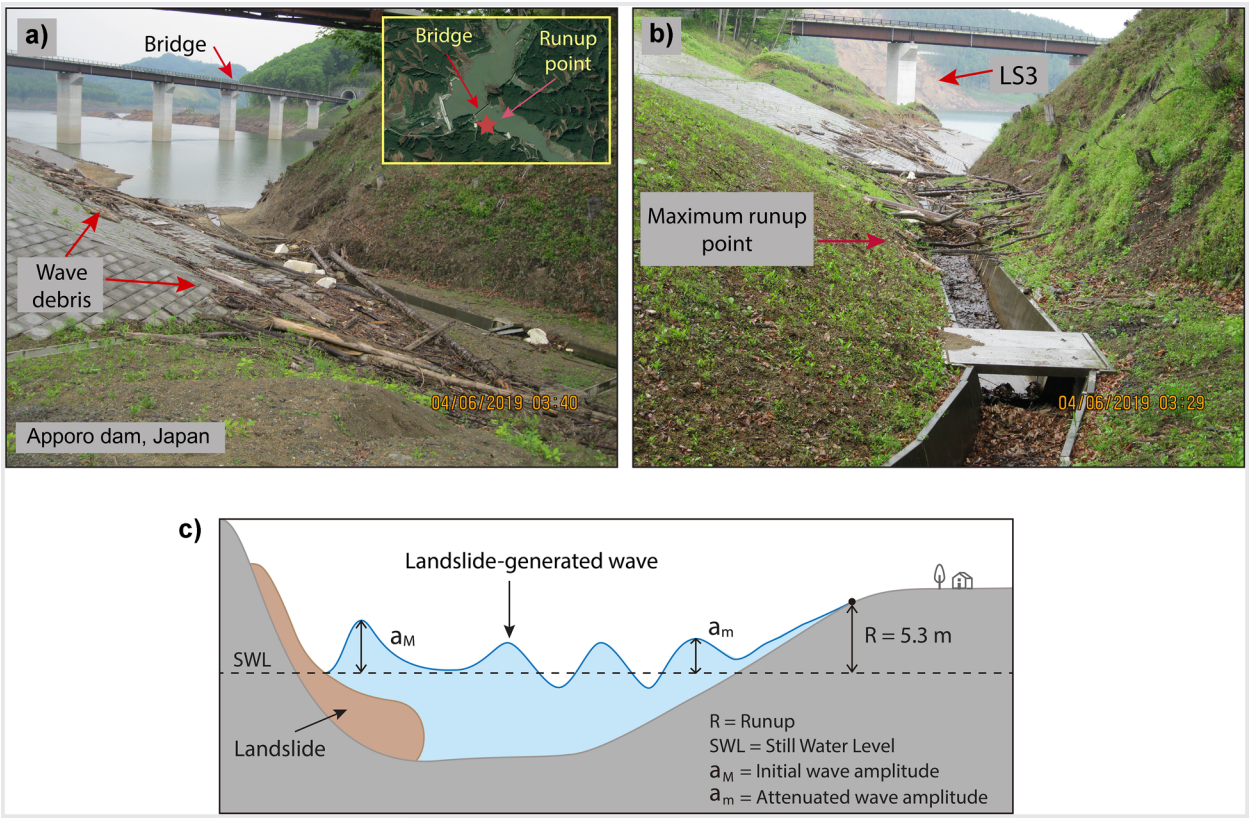

Fig. 8 Measurement of the runup of the landslide-generated waves in the Apporo dam reservoir following the September 2018 Hokkaido earthquake. **a**, **b** Runup measurement point showing the debris generated by landslide-generated wave. The inset at the upper-left of **a** shows the runup measurement point. **c** Sketch showing the definition of maximum initial wave amplitude (a_M), the attenuated wave amplitude due to propagation (a_m), and runup height (R)

The results of predictions for maximum initial wave amplitude (a_M), attenuated wave amplitude due to propagation (a_m), and runup height (R_1 and R_2) are presented in Table 2 indicating that the equations result in runup values in a wide range of

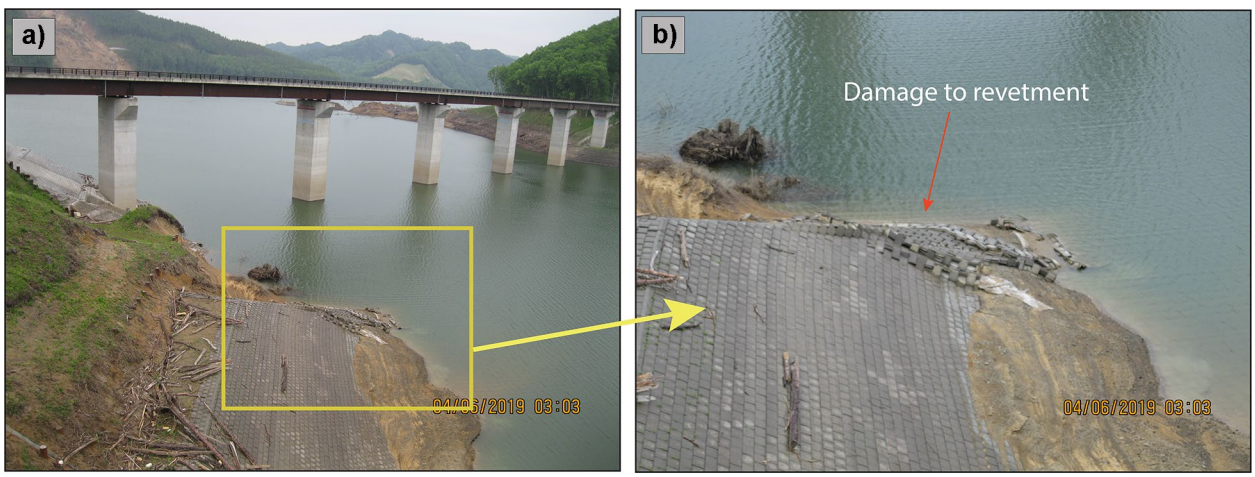

Fig. 9 Damage from the landslide-generated waves around the left bank of the Apporo dam reservoir following the September 2018 Hokkaido earthquake. This is the entrance of the opening that we measured runup (Fig. 8). **a** A photo from far showing the damaged reservoir bank revetment, the reservoir and the bridge passing through the reservoir. The box indicates the area enlarged in **b** of this figure. **b** A close-up view of the damaged area, which is the area shown in a box in **a**

Table 2 The maximum initial wave amplitude (a_M), the attenuated wave amplitude due to propagation (a_m), and runup height (R_1 and R_2) estimated from various empirical equations for the combination of three landsides of LS1, LS2, and LS3. The average value of drop heights for LS1, LS2 and LS3 is used for calculations

Empirical equations*	Landslide parameters**		a_M(m)	a_m(m)+	R_1(m) ++	R_2(m)#
	l_s(m)	b_s(m)				
$\frac{a_M}{h} = 0.25\left(\frac{v_s}{\sqrt{gh}}\right)^{1.4}\left(\frac{s}{h}\right)^{0.8}$	245.0	265.0	2.0	0.6	1.5	1.8
$\frac{a_M}{h} = 0.40\left(\frac{v_s}{\sqrt{gh}}\right)^{0.81}(s/h)^{0.40}(l_s/h)^{0.18}\tan^{0.15}\alpha$	245.0	265.0	7.9	2.3	8.2	7.2
$\frac{a_M}{h} = \frac{4}{9}\left[\frac{v_s}{\sqrt{gh}}\left(\frac{s}{h}\right)^{0.5}\left(\frac{m_s}{\rho_w b_s h^2}\right)^{0.25}\left(\cos\frac{6}{7}\alpha\right)^{0.5}\right]^{0.8}$	245.0	265.0	6.8	1.9	6.7	6.2
$\frac{a_M}{h} = 0.50\left[\left(\frac{v_s}{\sqrt{gh}}\right)^{1.00}\left(\frac{s}{h}\right)^{1.10}\left(\frac{m_s}{\rho_w b_s h^2}\right)^{1.00}\right]^{0.85}$	245.0	265.0	2.4	0.7	1.8	2.1
$\frac{a_M}{h} = 10^{\left[-1.25+0.71\log\left(0.5\frac{\rho_s}{\rho_w}\frac{v_s}{h^{\frac{3}{2}}}\frac{v_s^2}{gh}\right)\right]}$	245.0	265.0	39.5	11.2	60.8	41.2
$\frac{a_M}{h} = \left[0.398 + 0.076\left(V\left(\frac{v_s}{\sqrt{gh}}\right)^2\right)^{1.27}\right]\left(\frac{T_s}{V}\right)^{-0.26}\left(\frac{l_s}{s}\right)^{-0.125}\left(\frac{r}{h}\right)^{-0.48}$	245.0	265.0	11.4	Included	62.2	42.1
$\frac{a_M}{h} = 1.32\left(\frac{v_s}{\sqrt{gh}}\right)$	245.0	265.0	58.0	16.5	98.2	65.3
$\frac{a_M}{h} = 0.31\left(\frac{v_s}{\sqrt{gh}}\right)^{2.1}\left(\frac{s}{h}\right)^{0.6}\cos\theta\left(\frac{r}{h}\right)^{n}$	245.0	265.0	0.5	Included	1.3	1.6

*Developers of the equations are Fritz et al. (2004), Xue et al. (2019), Heller and Hager (2014), Heller and Spinneken (2015), Slingerland and Voight (1982), Ataie-Ashtiani and Nik-Khah (2008), Noda (1970), and Mohammed and Fritz (2012) for the first, second, third, fourth, fifth, sixth, seventh, and eighth equations, respectively.

**a_M, the maximum initial wave amplitude; a_m, the attenuated wave amplitude due to propagation; R_1 and R_2, and runup height; l_s, average length of three landslides of LS1, LS2, and LS3; b_s, sum of the width of three landslide (LS1, LS2, LS3); h, water depth (h= 27 m in this study); $v_s = \sqrt{2g\Delta z(1-\tan\delta\cot\alpha)}$, slide velocity at impact; Δz (=85 m), the drop height between the location of the slide centroid at rest and slide centroid reaching the initial water level; g, gravitational acceleration; δ (=12°), dynamic bed friction angle; α, slope angle of landslide (α= 20° in this study); s, slide thickness; l_s, slide length; m_s, slide mass; ρ_w (=1000 kg/m^3), water density; ρ_s (=1700 kg/m^3), slide density; r(=650 m), distance between the location of wave runup and impact point; θ (=10°), direction relative to landslide propagation; $T_s = 0.43V^{-0.27}\frac{v_s}{\sqrt{gh}}^{-0.66}(\sin\alpha)^{1.32}$ is the dimensionless slide underwater travel time; $V = V_s/b_s h^2$, dimensionless slide volume; Equation for v_s is from Kamphuis and Bowering (1970); $n = -1.2\left(\frac{v_s}{\sqrt{gh}}\right)^{0.25}\left(\frac{s}{h}\right)^{-0.02}\left(\frac{b_s}{h}\right)^{-0.33}$, based on Mohammed and Fritz (2012).

+For estimating attenuation of the waves due to propagation, we used the equation by Fritz et al. (2004): $\frac{a_m}{a_M} = \left[1+\frac{(x_M-r)}{h}\right]^{-0.4}$, where a_m is the attenuated maximum positive wave amplitude due to a propagation distance of r, x_M (=50 m) is the location of the maximum initial wave amplitude, and r (=650 m) is the propagation distance.

++Runup equation based on Synolakis (1987): $R_1 = 2.831h(\cot\beta)^{0.5}(a_m/h)^{1.25}$, where R_1 is runup, β is beach slope (β = 10° in this study), and a_m is the attenuated maximum positive wave amplitude due to propagation.

#Runup equation based on Evers and Boes (2019): $R_2 = 2a_m e^{0.4(\frac{a_m}{h})}(\frac{90^\circ}{\beta})^{0.2}$, where R_2 is runup, β = 10° in this study, and a_m is the attenuated maximum positive wave amplitude due to propagation..

1.3–98.2 m, whereas the measured runup in the field was 5.3 m. Among the examined empirical equations, those of Xue et al. (2019) and Heller and Hager (2014) give the closest predictions to the measured runup, with respective runup predictions of 7.2 m and 6.2 m. Some equations, such as Noda (1970), result in extreme overestimation, such as 98.2 m, which are far greater than the actual measurement. This could be partly because some of the equations used in Table 2 are based on 2D experiments, which are thought to overestimate the waves. It is useful to note that the two equations that we applied for runup predictions (Synolakis 1987; Evers and Boes 2019) yield values close to one another although that of Evers and Boes (2019) predicts slightly better. We note that the actual wave runup process is associated with 3D effects which implies that the wave propagates in various directions and undergoes transformation while propagating over irregular bathymetry. These phenomena introduce further challenges for applying empirical equations.

The analysis of wave prediction using existing empirical equations reveals that the measured runup height of 5.3 m (Fig. 8c) can be approximately reproduced by two equations of Xue et al. (2019) and Heller and Hager (2014) whereas other predictive equations are unsuccessful in reproducing the field measurement.

Discussions

The predictions of wave runup made by various existing empirical equations are divided by a couple of orders of magnitude (up to approximately hundred times) (Table 2). However, this is not a surprise because most empirical relationships are developed using limited laboratory data which are obtained under various limitations (e.g., Sabeti and Heidarzadeh 2020). Several reasons may contribute to such large uncertainties associated with the prediction of empirical equations, such as (i) lack of enough experimental database that could include a large number of data points (e.g., 1000 s of data points); (ii) the rather complicated mechanism of wave generation process by landslides which involves many factors such as water depth, type of the sliding materials, friction, rheology, speed and other factors; (iii) lack of enough actual field data that could help to further constrain empirical equations and improve their predictions as actual field data with real measurements are very limited; (iv) experimental studies are conducted in small lab scales which are subject to various scale and model effects (e.g., Heller et al. 2008); and (v) propagation of the wave over actual irregular bathymetries, which are not properly represented by empirical predictive equations (e.g., Franco et al. 2021). Therefore, efforts in various fronts need to be made to further improve the qualities of predictive relationships including additional experimental and field data. Our field data from the Apporo dam landslide-generated waves could provide data for improving the qualities of empirical equations in the future.

Landslide-generated waves are real threats to dams' safety worldwide and must be taken seriously. They can endanger the safety of dams and the surrounding communities as evidenced by the Vajont dam disaster (Italy) in 1963 (Barla and Paronuzzi 2013; Roberts et al. 2014). In particular, even moderate-size landslides could be of high safety risks for situations when the reservoir water level is closer to the dam crest elevation. Therefore, although the 2018 Apporo dam landslide-generated wave did not make large destruction or overtopping as the reservoir water level was significantly lower than the normal water level at the time of the event, it must be considered as a warning call for the dam authorities to carefully assess unstable slopes around the dam reservoir, estimate their potential sizes, prepare emergency guidelines in case of slope failures, and consider stabilization works on the unstable slopes as much as possible. It is possible that a larger-magnitude earthquake could trigger a much larger landslide with more severe consequences.

Conclusions

The destructive and rare combination of the September 2018 Typhoon Jebi and M_w 6.6 Hokkaido earthquake led to the generation of nearly 6,000 landslides in Hokkaido (Japan), where several of them slid into the Apporo dam reservoir and produced landslide-generated waves. We conducted field surveys of the landslides around the Apporo dam and documented six landslides in the vicinity of the dam body. The largest of these landslides has a length and maximum width of 330 m and 140 m, respectively, with an estimated volume of 71,400 m^3. We identified impacts of a landslide-generated wave around the left abutment of the dam which caused some damage to the concrete revetment. The surveyed runup height of this wave was 5.3 m, which was reproduced employing two independent empirical equations and using landslide parameters although we acknowledge that such applications of empirical predictive equations are associated with uncertainties. By considering the locations of the landslides and their potential propagation paths, we speculate that possibly three of them contributed to the measured wave runup. This landslide-generated wave was not a major risk for the dam's safety, but it could have had serious consequences if the reservoir water level was closer to the dam crest elevation or if the size of the landslides was larger. Although two independent empirical equations successfully reproduced our surveyed runup, some others failed which can be attributed to the large uncertainties associated with predictions made by empirical equations. The field-measured data provided in this research can be used to improve the quality of predictions made by empirical equations. Our field data also serves as a call for strengthening safety of dams to landslide-generated waves in reservoirs.

Acknowledgements

A number of figures were drafted using the GMT software (Wessel and Smith 1998). We thank the engineers at the Apporo dam (Hokkaido, Japan) for assisting us during the field surveys and the Hokkaido Prefecture Authorities for providing reservoir water level data. We are grateful to the Editor, one anonymous reviewer, and Dr Nicholas J. Roberts for their constructive and useful review comments.

Funding

This research is funded by the Great Britain Sasakawa Foundation (http://www.gbsf.org.uk/) under grant number 5542 (2018), and the Royal Society, the UK, grant number CHL/R1/180173. We also acknowledge funding from the open funding of State Key Lab of Hydraulics and Mountain River Engineering, Sichuan University, grant number SKHL2101.

Availability of data and materials

All data used in this research are provided in the body of the article.

Code availability

Not applicable to this study.

Declarations

Conflict of interest The authors declare no competing interests.

References

Adams K, Heidarzadeh M (2021) A multi-hazard risk model with cascading failure pathways for the Dawlish (UK) railway using historical and contemporary data. Int J Disaster Risk Reduct 56:102082. https://doi.org/10.1016/j.ijdrr.2021.102082

Alcantara-Ayala I, Dominguez-Morales L (2008) The San Juan de Grijalva catastrophic landslide, Chiapas, Mexico: lessons learnt. Edited by: Casagli N, Fanti R, Tofani V. Proc First World Landslide Forum

Aimaiti Y, Liu W, Yamazaki F, Maruyama Y (2019) Earthquake-induced landslide mapping for the 2018 Hokkaido Eastern Iburi Earthquake Using PALSAR-2 data. Remote Sensing 11(20):2351

Ataie-Ashtiani B, Yavari-Ramshe S (2011) Numerical simulation of wave generated by landslide incidents in dam reservoirs. Landslides 8(4):417–432

Ataie-Ashtiani B, Nik-Khah A (2008) Impulsive waves caused by subaerial landslides. Environ Fluid Mech 8(3):263–280

Barla G, Paronuzzi P (2013) The 1963 Vajont landslide: 50th anniversary. Rock Mech Rock Eng 46(6):1267–1270

Bosa S, Petti M (2011) Shallow water numerical model of the wave generated by the Vajont landslide. Environ Model Softw 26(4):406–418

Chang M, Zhou Y, Zhou C, Hales TC (2021) Coseismic landslides induced by the 2018 M w 6.6 Iburi, Japan, Earthquake: spatial distribution, key factors weight, and susceptibility regionalization. Landslides 18(2):755–772

Chen G, Xia M, Thuy DT, Zhang Y (2021) A possible mechanism of earthquake-induced landslides focusing on pulse-like ground motions. Landslides 18(5):1641–1657

Dziewonski AM, Chou T-A, Woodhouse JH (1981) Determination of earthquake source parameters from waveform data for studies of global and regional seismicity. J Geophys Res 86(B4):2825–2852. https://doi.org/10.1029/JB086iB04p02825

Ekström G, Nettles M, Dziewonski AM (2012) The global CMT project 2004–2010: Centroid-moment tensors for 13,017 earthquakes. Phys Earth Planet Inter 200–201:1–9. https://doi.org/10.1016/j.pepi.2012.04.002

Ersoy H, Karahan M, Gelişli K, Akgün A, Anılan T, Sünnetci MO, Yahşi BK (2019) Modelling of the landslide-induced impulse waves in the Artvin Dam reservoir by empirical approach and 3D numerical simulation. Eng Geol 249:112–128

Evers FM, Boes RM (2019) Impulse Wave Runup on Steep to Vertical Slopes. Journal of Marine Science and Engineering 7(1):8. https://doi.org/10.3390/jmse7010008

Evers F, Heller V, Fuchs H, Hager WH, Boes R (2019a) Landslide-generated Impulse Waves in Reservoirs: Basics and Computation. VAW-Mitteilungen 254

Evers FM, Hager WH, Boes RM (2019b) Spatial Impulse Wave Generation and Propagation. J Waterw Port Coast Ocean Eng 145:04019011

Franco A, Schneider-Muntau B, Roberts NJ, Clague JJ, Gems B (2021) Geometry-based preliminary quantification of landslide-induced impulse wave attenuation in mountain lakes. Appl Sci 11(24):11614. https://doi.org/10.3390/app112411614

Fritz HM, Kalligeris N, Borrero JC, Broncano P, Ortega E (2008) The 15 August 2007 Peru tsunami runup observations and modeling. Geophys Res Lett 35(10)

Fritz HM, Hager WH, Minor HE (2004) Near field characteristics of landslide generated impulse waves. J Waterw Port Coast Ocean Eng 130(6):287–302

Gill JC, Malamud BD (2016) Hazard interactions and interaction networks (cascades) within multi-hazard methodologies. Earth System Dynamics 7(3):659–679

Heidarzadeh, M., Feizi, S. (2022). A cascading risk model for the failure of the concrete spillway of the Toddbrook dam, England during the August 2019 flooding. Int J Disast Risk Reduct 80:103214. https://doi.org/10.1016/j.ijdrr.2022.103214

Heidarzadeh, M., Gusman, A., Ishibe, T., Sabeti, R., Šepić, J. (2022). Estimating the eruption-induced water displacement source of the 15 January 2022 Tonga volcanic tsunami from tsunami spectra and numerical modelling. Ocean Eng 261:112165. https://doi.org/10.1016/j.oceaneng.2022.112165

Heidarzadeh M, Teeuw R, Day S, Solana C (2018) Storm wave runups and sea level variations for the September 2017 Hurricane Maria along the coast of Dominica, eastern Caribbean Sea: evidence from field surveys and sea level data analysis. Coast Eng J 60(3):371–384. https://doi.org/10.1080/21664250.2018.1546269

Heidarzadeh M, Putra PS, Nugroho HS, Rashid DBZ (2020) Field survey of tsunami heights and runups following the 22 December 2018 Anak Krakatau volcano tsunami, Indonesia. Pure Appl Geophys 177:4577–4595. https://doi.org/10.1007/s00024-020-02587-w

Heidarzadeh M, Muhari A, Wijanarto AB (2019) Insights on the source of the 28 September 2018 Sulawesi tsunami, Indonesia based on spectral analyses and numerical simulations. Pure Appl Geophys 176:25–43. https://doi.org/10.1007/s00024-018-2065-9

Heidarzadeh M, Rabinovich AB (2021) Combined Hazard of Typhoon-Generated Meteorological Tsunamis and Storm Surges along the Coast of Japan. Nat Hazards 106:1639–1672. https://doi.org/10.1007/s11069-020-04448-0

Heidarzadeh M, Satake K (2015) Source properties of the 17 July 1998 Papua New Guinea tsunami based on tide gauge records. Geophys J Int 202(1):361–369. https://doi.org/10.1093/gji/ggv145

Heller V, Hager WH (2010) Impulse product parameter in landslide generated impulse waves. J Waterw Port Coast Ocean Eng 136:145–155

Heller V, Hager WH (2014) A universal parameter to predict subaerial landslide tsunamis? J Mar Sci Eng 2(2):400–412

Heller V, Spinneken J (2015) On the effect of the water body geometry on landslide–tsunamis: Physical insight from laboratory tests and 2D to 3D wave parameter transformation. Coast Eng 104:113–134

Heller V, Hager WH, Minor HE (2008) Scale effects in subaerial landslide generated impulse waves. Exp Fluids 44(5):691–703

Hermanns RL, Oppikofer T, Roberts NJ, Sandøy G (2014) Catalogue of historical displacement waves and landslide-triggered tsunamis in Norway. In: G. Lollino et al. (eds.), Engineering Geology for Society and Territory – Volume 4. https://doi.org/10.1007/978-3-319-08660-6_13

Huang B, Yin Y, Liu G, Wang S, Chen X, Huo Z (2012) Analysis of waves generated by Gongjiafang landslide in Wu Gorge, three Gorges reservoir, on November 23, 2008. Landslides 9(3):395–405

Japan Commission on Large Dams (2018) Dams in Japan: overview 2018. Online materials at: https://jcold.or.jp/cm/wp-content/uploads/2020/01/Dams-in-Japan-2018-web%E7%94%A8.pdf (page last accessed on 18th May 2021)

Kamphuis JW, Bowering RJ (1970) Impulse waves generated by landslides. In: Proceedings of the 12th Coastal Engineering Conference, ASCE, Reston Va. 1 575–588

Katsumata K, Ichiyanagi M, Ohzono M, Aoyama H, Tanaka R, Takada M, Yamaguchi T, Okada K, Takahashi H, Sakai S, Matsumoto S, Okada T, Matsuzawa T, Hirano S, Terakawa T, Horikawa S, Kosuga M, Katao H, Iio Y, Nagaoka A, Tsumura N, Ueno T, the Group for the Aftershock Observations of the 2018 Hokkaido Eastern Iburi Earthquake (2019) The 2018 Hokkaido Eastern Iburi earthquake (M_{JMA}= 6.7) was triggered by a strike-slip faulting in a stepover segment: insights from the aftershock distribution and the focal mechanism solution of the main shock. Earth Planets Space 71:53. https://doi.org/10.1186/s40623-019-1032-8

Le TA, Takagi H, Heidarzadeh M, Takata Y, Takahashi A (2019) field surveys and numerical simulation of the 2018 Typhoon Jebi: impact of high waves and storm surge in semi-enclosed Osaka Bay. Japan Pure and Applied Geophysics 176(10):4139–4160. https://doi.org/10.1007/s00024-019-02295-0

Li R, Wang F, Zhang S (2020) Controlling role of Ta-d pumice on the coseismic landslides triggered by 2018 Hokkaido Eastern Iburi Earthquake. Landslides 17(5):1233–1250
Liu B, Siu YL, Mitchell G (2016) Hazard interaction analysis for multi-hazard risk assessment: a systematic classification based on hazard-forming environment. Nat Hazard 16(2):629–642
Lu P, Shi W, Wang Q, Li Z, Qin Y, Fan X (2021) Co-seismic landslide mapping using Sentinel-2 10-m fused NIR narrow, red-edge, and SWIR bands. Landslides 1–21
Lyddon CE, Brown JM, Leonardi N, Saulter A, Plater AJ (2019) Quantification of the uncertainty in coastal storm hazard predictions due to wave-current interaction and wind forcing. Geophys Res Lett 46(24):14576–14585
Miyagi T, Yamashina S, Esaka F, Abe S (2011) Massive landslide triggered by 2008 Iwate-Miyagi inland earthquake in the Aratozawa Dam area, Tohoku. Japan Landslides 8(1):99–108
Muhari A, Heidarzadeh M, Susmoro H, Nugroho HD, Kriswati E, Supartoyo Wijanarto AB, Imamura F, Arikawa T (2019) The December 2018 Anak Krakatau volcano tsunami as inferred from post-tsunami field surveys and spectral analysis. Pure Appl Geophys 176:5219–5233. https://doi.org/10.1007/s00024-019-02358-2
McCulloch DS (1966) Slide-induced waves, seiching, and ground fracturing caused by the earthquake of March 27, 1964, at Kenai Lake, Alaska. Geol Surv Prof Pap 543-A
McFall BC, Fritz HM (2016) Physical modelling of tsunamis generated by three-dimensional deformable granular slides on planar and conical island slopes. Proceedings of Royal Society London A 472(2188):20160052
Mohammed F, Fritz HM (2012) Physical modeling of tsunamis generated by three-dimensional deformable granular landslides. J Geophys Res Oceans 117 (C11). https://doi.org/10.1029/2011JC007850
Noda E (1970) Water waves generated by landslides. J Waterw Harb Coast Eng Div 96(4):835–855
Omira R, Dogan GG, Hidayat R, Husrin S, Prasetya G, Annunziato A, Proietti C et al (2019) The September 28th, 2018, tsunami in Palu-Sulawesi, Indonesia: A post-event field survey. Pure Appl Geophys 176(4):1379–1395
Oppikofer T, Hermanns RL, Roberts NJ, Böhme M (2019) SPLASH: semi-empirical prediction of landslide-generated displacement wave run-up heights. Geological Society, London, Special Publications 477(1):353–366. https://doi.org/10.1144/SP477.1
Osanai N, Yamada T, Hayashi SI, Kastura SY, Furuichi T, Yanai S, Murakami Y, Miyazaki T, Tanioka Y, Takiguchi S, Miyazaki M (2019) Characteristics of landslides caused by the 2018 Hokkaido Eastern Iburi Earthquake. Landslides 16(8):1517–1528
Panizzo A, Girolamo PD, Risio MD, Maistri A, Petaccia A (2005) Great landslide events in Italian artificial reservoirs. Nat Hazard 5(5):733–740
Roberts NJ, McKillop RJ, Lawrence MS, Psutka JF, Clague JJ, Brideau MA, Ward BC (2013) Impacts of the 2007 landslide-generated tsunami in Chehalis Lake, Canada. In: Landslide science and practice (pp. 133–140). Springer, Berlin, Heidelberg. https://doi.org/10.1007/978-3-642-31319-6_19
Robert NJ, McKillop R, Hermanns RL, Clague JJ, Oppikofer T (2014) Preliminary Global Catalogue of Displacement Waves from Subaerial Landslides. In: Proc. Third World Landslide Forum. K. Sassa et al. (eds.). Landslide Sci Safer Geoenviron 3. https://doi.org/10.1007/978-3-319-04996-0_104
Sabeti R, Heidarzadeh M (2020) Semi-empirical predictive equations for the initial amplitude of submarine landslide-generated waves: applications to 1994 Skagway and 1998 Papua New Guinea tsunamis. Nat Hazards 103:1591–1611. https://doi.org/10.1007/s11069-020-04050-4
Savage BM, Johnson MC (2001) Flow over ogee spillway: Physical and numerical model case study. J Hydraul Eng 127(8):640–649
Slingerland R, Voight B (1982) Evaluating hazard of landslide-induced water waves. Journal of the Waterway, Port, Coastal and Ocean Division 108(4):504–512
Schnitter G (1964) Die Katastrophe von Vaiont in Oberitalien. Wasser- Und Energiewirtschaft 56(2/3):61–69
Schuster RL, Wieczorek GF (2002) Landslide triggers and types. In: Proceedings of the 1st European Conference on Landslides, Editors: J. Rybář, J. Stemberk, P. Wagner, Prague, Czech Republic 59–78, Balkema, Tokyo
Synolakis CE (1987) The runup of solitary waves. J Fluid Mech 185:523–545
Takagi H, Takahashi A (2021) Short-fetch high waves during the passage of 2019 Typhoon Faxai over Tokyo Bay. Front Earth Sci 15(2)
Takagi H, Pratama MB, Kurobe S, Esteban M, Aránguiz R, Ke B (2019) Analysis of generation and arrival time of landslide tsunami to Palu City due to the 2018 Sulawesi earthquake. Landslides 16(5):983–991
Tsuji Y, Satake K, Ishibe T, Kusumoto S, Harada T, Nishiyama A, Kim HY, Ueno T, Murotani S, Oki S, Sugimoto M, Tomari J, Heidarzadeh M, Watada S, Imai K, Choi BH, Yoon SB, Bae JS, Kim KO, Kim HW (2011) Field surveys of tsunami heights from the 2011 Off the Pacific Coast of Tohoku, Japan, earthquake. Bulletin of the Earthquake Research Institute University of Tokyo 86:29–279 (in Japanese with English abstract)
Vacondio R, Mignosa P, Pagani S (2013) 3D SPH numerical simulation of the wave generated by the Vajont rockslide. Adv Water Resour 59(9):146–156
Wang F, Fan X, Yunus AP, Subramanian SS, Alonso-Rodriguez A, Dai L, Xu Q, Huang R (2019) Coseismic landslides triggered by the 2018 Hokkaido, Japan (M w 6.6), earthquake: spatial distribution, controlling factors, and possible failure mechanism. Landslides 16(8):1551–1566
Wessel P, Smith WHF (1998) New improved version of Generic Mapping Tools released. EOS Trans Am Geophys Union 79(47):579–579
Xue H, Ma Q, Diao M, Jiang L (2019) Propagation characteristics of subaerial landslide-generated impulse waves. Environ Fluid Mech 19(1):203–230
Yamagishi H, Yamazaki F (2018) Landslides by the 2018 Hokkaido Iburi-Tobu Earthquake on September 6. Landslides 15(12):2521–2524
Yin YP, Huang B, Chen X, Liu G, Wang S (2015) Numerical analysis on wave generated by the Qianjiangping landslide in Three Gorges Reservoir. China Landslides 12(2):355–364
Zhang S, Li R, Wang F, Iio A (2019) Characteristics of landslides triggered by the 2018 Hokkaido Eastern Iburi earthquake. Northern Japan Landslides 16(9):1691–1708
Zhou JW, Xu FG, Yang XG, Yang YC, Lu PY (2016) Comprehensive analyses of the initiation and landslide-generated wave processes of the 24 June 2015 Hongyanzi landslide at the Three Gorges Reservoir. China Landslides 13(3):589–601

Mohammad Heidarzadeh (✉)
Department of Architecture and Civil Engineering, University of Bath, Bath BA2 7AY, UK
Email: mhk58@bath.ac.uk

Hiroko Miyazaki · Ramtin Sabeti
Department of Civil & Environmental Engineering, Brunel University London, Uxbridge UB8 3PH, UK

Takeo Ishibe
Association for the Development of Earthquake Prediction, 101-0064 Tokyo, Japan

Hiroshi Takagi
School of Environment and Society, Tokyo Institute of Technology, Tokyo 152-8550, Japan